Supplement of Atmos. Meas. Tech., 14, 5913–5923, 2021
https://doi.org/10.5194/amt-14-5913-2021-supplement

Atmospheric Measurement Techniques
Open Access
EGU

Supplement of

Effects of aerosol size and coating thickness on the molecular detection using extractive electrospray ionization

Chuan Ping Lee et al.

Correspondence to: Imad El Haddad (imad.el-haddad@psi.ch), Dongyu Wang (dongyu.wang@psi.ch), and Jay G. Slowik (jay.slowik@psi.ch)

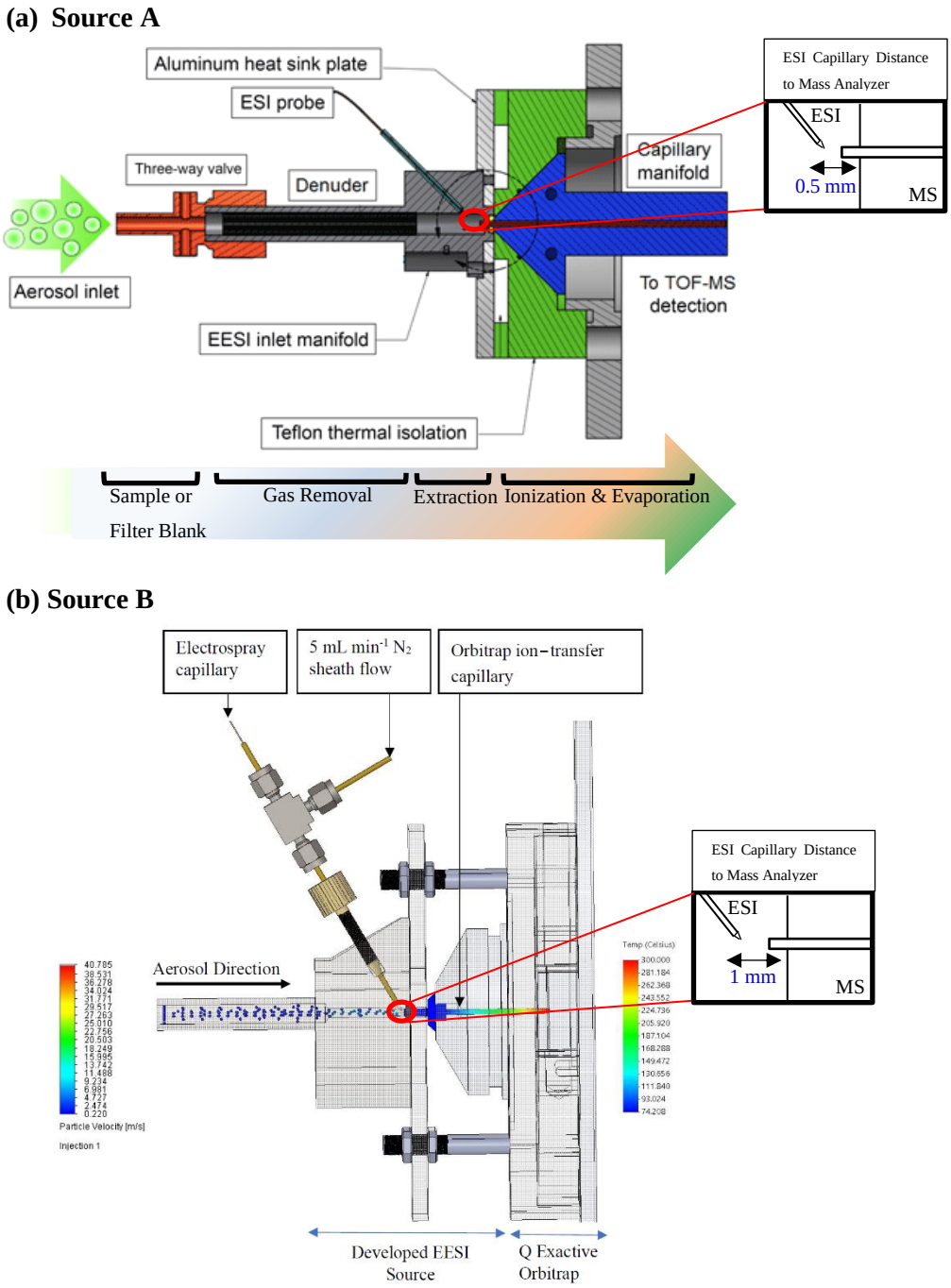

Figure S1. (a) EESI-TOF inlet compatible with the Tofwerk TOF system. (b) EESI-Orbitrap inlet compatible with the Thermo Fischer Scientific Orbitrap and Tofwerk TOF systems. Note: The charcoal denuder is not included in the picture (b). Source A was developed by the Laboratory of Atmospheric Chemistry, Paul Scherrer Institute, Switzerland (LAC-PSI) in collaboration with TOFWERK AG, Switzerland. Source B was development by LAC-PSI in collaboration with IRCELYON, France (Lopez-Hilfiker et al., 2019; Lee et al., 2020). The approximate distance between the tip of the spray capillary and the heated ion transfer tube at the mass spectrometer interface is shown in the insets. The ESI probes of the EESI sources have the similar inclination of 30° from the horizontal axis at the mass analyzer capillary. Both EESI sources were deployed on the same mass analyzer with the same sampling flow of 0.8 L min^{-1} for the whole experiment.

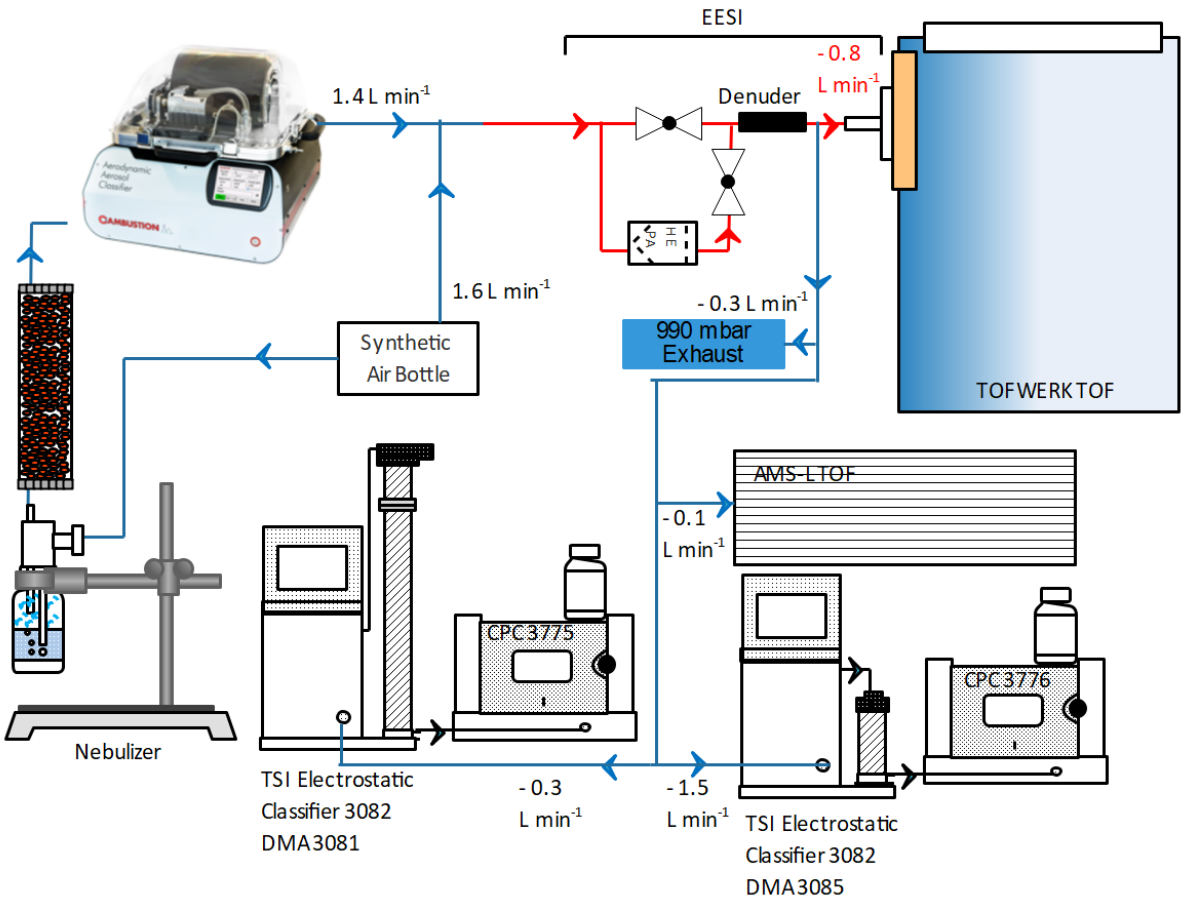

Figure S2. Schematic of the experimental setup for size-dependent sensitivity of the EESI-TOF. Red lines indicate the schematic layout of the EESI-TOF ionization inlet with additional two two-way valves and tubing manifolds prior to the electrospray ionization region for two different settings: (1) with charcoal denuder only and (2) with charcoal denuder and HEPA filter. Blue lines indicate the setup, which is used for the size-dependent sensitivity experiment.

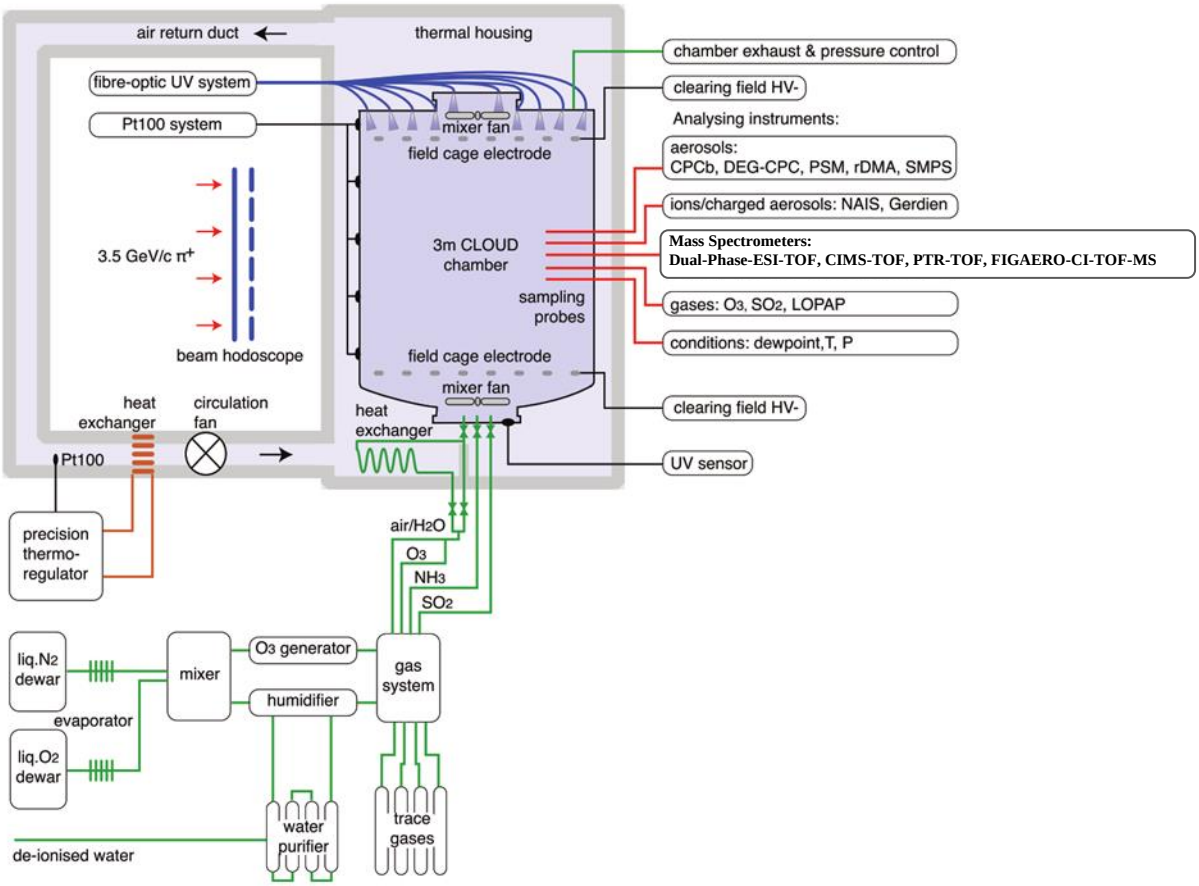

Figure S3. Schematic diagram of the CLOUD-14 experiment at CERN, modified from Kirkby et al. (2011).

CLOUD chamber. The CLOUD facility provides suitable conditions to study new particle formation (NPF) under atmospherically relevant conditions, using the well-characterized cylindrical stainless-steel chamber (CLOUD chamber) with ultra-low contamination level and equipped with state-of-the art instrumentation (see Figure S3). The CLOUD chamber is an electro-polished stainless-steel cylindrical chamber of 3 m diameter, ~4 m height and 26.1 m^3 inner volume, positioned inside a thermal housing (Kirkby et al., 2011). A continuous flow of synthetic air from evaporation of cryogenic liquid nitrogen and liquid oxygen at a volume mixing ratio of 79:21 is injected to the chamber to balance the experiment sample flow. When all the instruments are connected to the CLOUD facility, the total air flow rate is typically 270 L min^{-1}, resulting in a dilution lifetime of 1.6 h in the chamber. Humidity of the chamber is adjusted by passing the air through a Nafion® humidifier using ultrapure water (18 MΩ cm, Millipore Corporation).

The relative humidity of the chamber is determined by dew point mirrors (EdgeTech). Ozone (O_3) is generated by exposing a small fraction of the air through a quartz tube surrounded by UVC lamps (wavelength <240 nm) and added to the inlet chamber flow. For NPF experiments, the chamber is operated at 5 mbar above atmospheric pressure using a pressure regulated valve. Two counter-rotating stainless-steel fans are mounted on the roof and bottom of the chamber to enable a uniform mixing inside the chamber. Under typical NPF experimental conditions, the fans are operated with 12% fan speed, resulting in a wall loss lifetime of 0.002 s^{-1} for sulfuric acid. A typical experiment in CLOUD is running in continuous mode, so precursors are constantly injected into the chamber. An

experiment starts when the particle concentration inside the chamber is low enough for the measurement and precursor gases such as SO_2 and / or volatile organic compounds (VOCs) have reached the intended concentration. Chemical reactions start by turning on UV lights or by mixing VOCs with oxidants such as ozone.

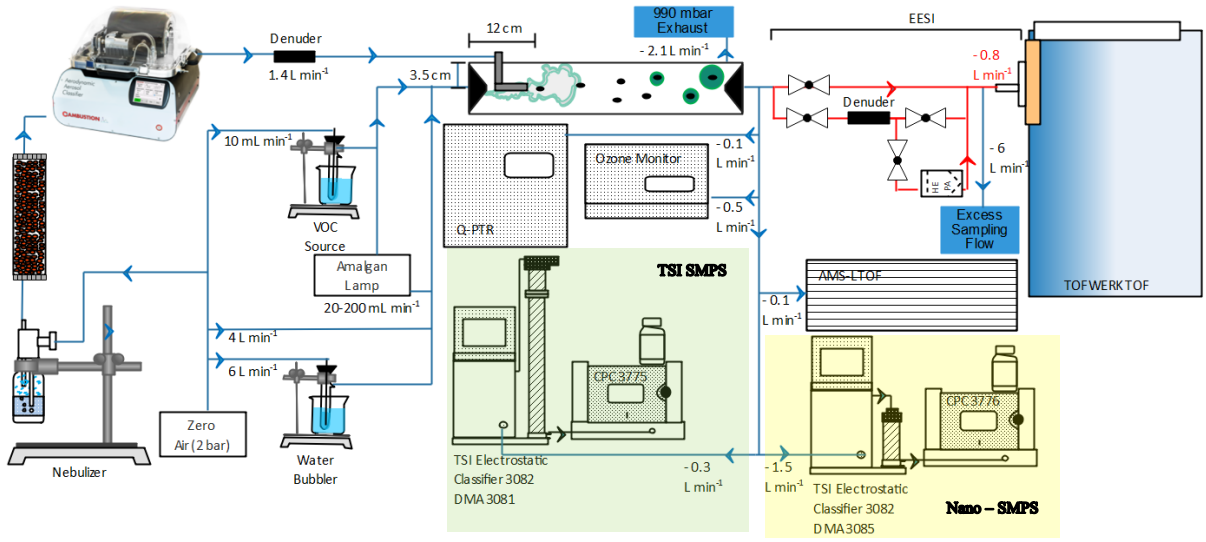

Figure S4. Schematic of the experimental setup for coating experiments using α-pinene oxidation products from a flow tube reactor. Inorganic particles (NH_4NO_3) are injected into the flow tube which act as condensation sink for the low-volatility oxidation products. Red lines indicate the schematic layout of the EESI-TOF ionization inlet with additional valve and tubing manifolds prior to the electrospray ionization region for three different settings: (1) open straight tube (without denuder and HEPA filter), (2) with charcoal denuder only, (3) with charcoal denuder and HEPA filter. Blue lines indicate the setup that is used for the coating experiment.

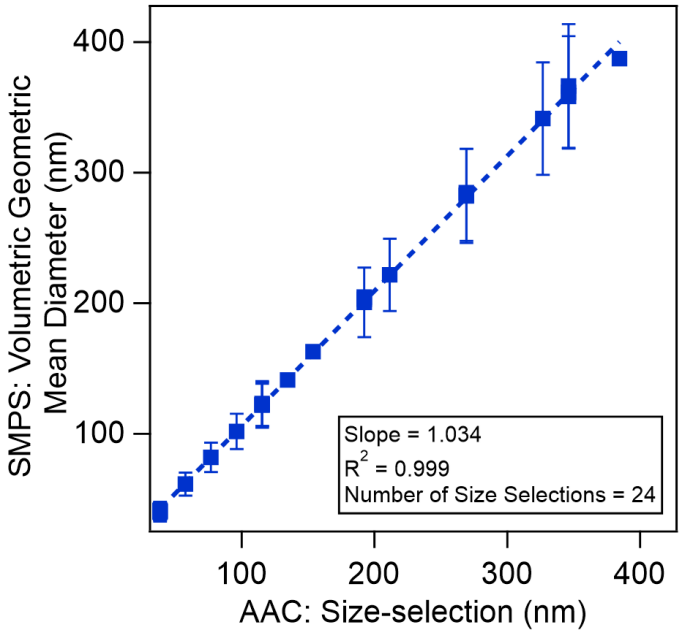

Figure S5. Measured volumetric geometric mean diameter by the SMPS as a function of selected size by the Aerosol Aerodynamic Classifier for levoglucosan particles. The SMPS measurement was corrected by applying the ion mobility ratio for air, which is 1.2/1.4. The AAC aerodynamic diameter was corrected according to the density of levoglucosan described below. The full width at half maximum (FWHM) of the measured particle size distribution by the SMPS is indicated by the *y*-axis uncertainty marker. The blue dotted-line indicates the linear fit with goodness of fit R^2 = 0.999.

For spherical particles, the aerodynamic diameter D_{ae} is defined as

$$D_{ae} = D_P \sqrt{\frac{\rho_P C_c(D_P)}{\rho_0 C_c(D_{ae})}} \quad \text{(Eq. S1)}$$

where $C_c(D)$ is the Cunningham slip correction factor applied to diameter D_p and D_{ae}, D_p is the diameter measured by a differential mobility particles sizer, ρ_0 = 1000 kg m^{-3} and ρ_P the density of the particle. To simplify the relationship shown in Figure S5,

$$\frac{D_P}{D_{ae}} = \sqrt{\frac{\rho_0}{\rho_P}} \quad \text{(Eq. S2)}$$

For the case of levoglucosan particles ρ_P = 1690 kg m^{-3}, the ratio of $\sqrt{\frac{\rho_0}{\rho_P}}$ = 0.769. After the correction of the aerodynamic diameters using levoglucosan density, the slope measured in Figure S5 is within an uncertainty of 5%.

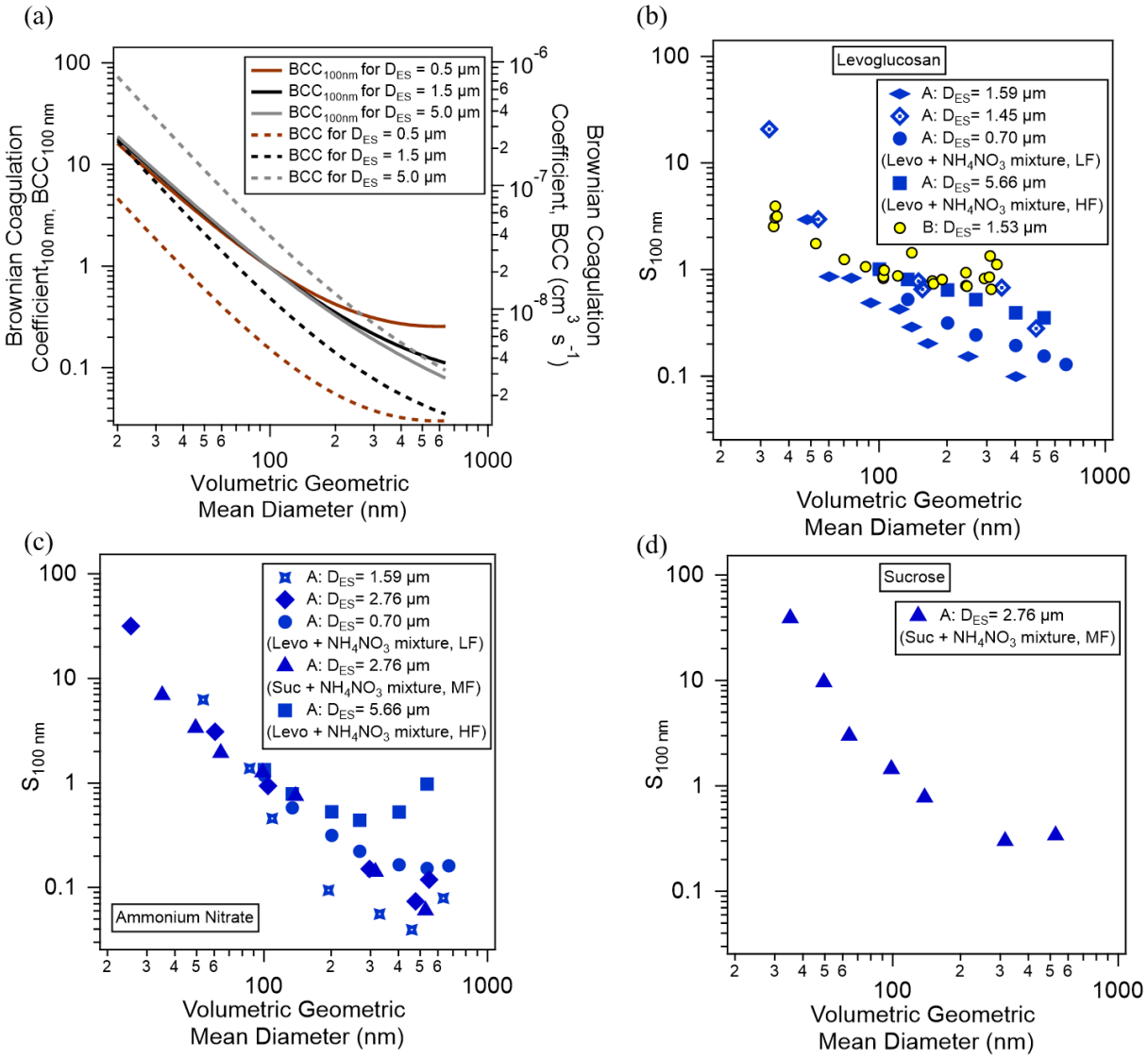

Figure S6. (a) Brownian coagulation coefficient (BCC) in cm^3 s^{-1} calculated assuming different parent electrospray droplet diameters (D_{ES}). The particle diameter is plotted along the *x*-axis. The D_{ES} values were chosen to cover the expected range (0.5 µm and 5.0 µm) and median (~1.5 µm) sizes of the actual electrospray droplet generated in this study (Table S3). D_{ES} is the electrospray parent droplet diameters that were estimated using scaling laws shown in Figure S7, assuming that the ES is operating in the Taylor cone jet mode (Gañán-Calvo et al., 2018). As done in-text for the measured sensitivities, the normalized BCC values (relative to that for 100 nm particle), BCC$_{100nm}$ are also shown. (b-d) size-dependent sensitivity measurements using individual and internally-mixed (mixture) chemical standards, i.e. (b) levoglucosan, (c) NH_4NO_3 and (d) sucrose. A and B denote the types of the EESI source used as depicted in Figure S1. The estimated D_{ES} value for a given the experimental condition (Table S2) is also shown in the legends. LF, MF and HF denote low, medium and high ES capillary flow as tabulated in Table S2. The mass concentration for internally mixed levoglucosan and NH_4NO_3 particles with D_p > 100 nm were measured by an LTOF-AMS.

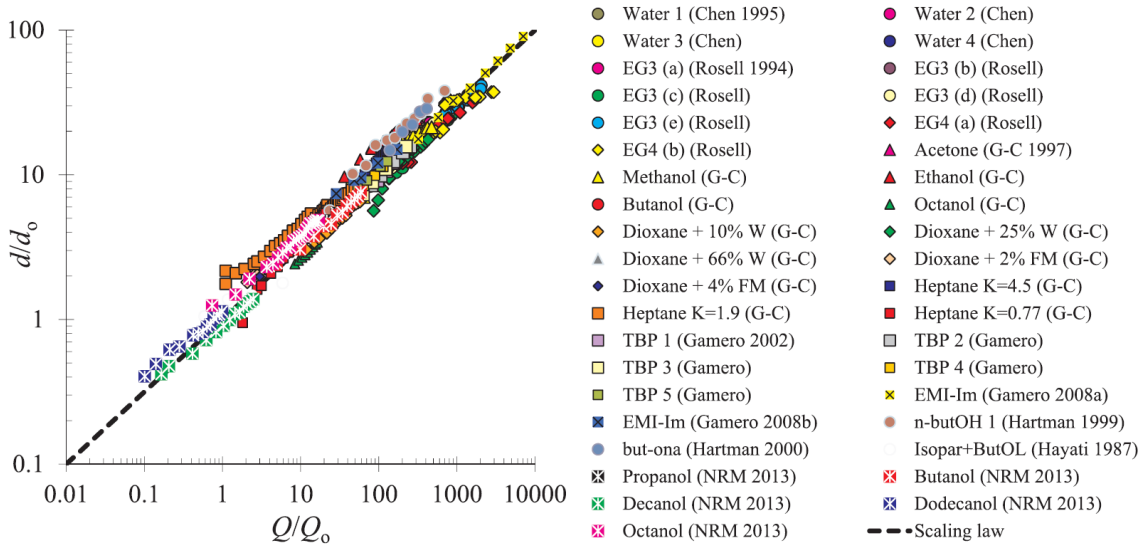

Figure S7. Scaling laws for predicting the orders of magnitude of the size *d* of the emitted ES charged droplet based on the flow rate *Q* for 39 types of electrospray working solutions. The predicted diameter *d* is denoted as $d = d_0\sqrt{Q/Q_0}$ (Gañán-Calvo et al., 2018).

D_{ES} shown in Figure S6 is calculated by from *Q*, Q_0 and d_0. *Q* is the calculated flow rate using the Hagen-Poiseuille equation:

$$Q = \frac{\Delta p \pi R^4}{8\mu L} \quad \text{(Eq. S3)}$$

where Δp is the pressure difference applied to the ES bottle reservoir, *R* is the inner radius of the ES capillary, *L* is the length of the ES capillary (80 cm) and μ is the dynamic viscosity of the ES working solution. The dynamic viscosity of H_2O:ACN (50:50 v/v) and H_2O at 25 ˚C are 0.65 and 0.89 mPa s, respectively. See Table S1 for other variables. Q_0 and d_0 are defined as

$$Q_0 = \sigma\varepsilon_0/(\rho K)$$
$$d_0 = [\sigma\varepsilon_0^2/\rho K^2]^{1/3} \quad \text{(Eq. S4)}$$

where σ is the surface tension, ρ is the density and *K* is the electrical conductivity of the electrospray working solutions.

Table S1. Physical properties of the electrospray solvents.

Physical Properties of the Electrospray Solvents			
Types of ES Solvent	Surface tension σ (N m^{-1})	Volumetric Density ρ (kg m^{-3})	Electrical Conductivity K (S m^{-1})
H_2O:ACN (50:50 v/v)	0.0514	842.54	0.000252
H_2O	0.072	997	0.0005

When all the variables are determined, D_{ES} is estimated as (Gañán-Calvo et al., 2016, 2018)

$$D_{ES} = d_0\sqrt{Q/Q_0}. \quad \text{(Eq. S5)}$$

Table S2. Size dependence experiments for different chemicals, EESI source and ES operating parameters. Levo#, AN# and Suc# indicate different levoglucosan, NH_4NO_3 and sucrose experiment runs, respectively.

Index no.	**EESI Source Designs**	**ES voltage (kV)**	**ES pressure (mbar)**	**ES capillary inner diameter (μm)**	**ES solution**	**Nebulization solution**	**ES Flow Rate, Q (nL min^{-1})**
Levo1 + AN1	A	2.6	200	50	H_2O:ACN (50:50 v/v)	Mixed	354
Levo2 + AN2	A	2.9	800	100	H_2O:ACN (50:50 v/v)	Mixed	22655
Levo3	A	2.95	200 - 400	75	H_2O:ACN (50:50 v/v)	Single	1792-3584
Levo4	A	2.88	200 - 400	75	H_2O	Single	1309-2617
AN3	A	2.95	200 - 400	75	H_2O:ACN (50:50 v/v)	Single	1792-3584
AN4 + Suc1	A	2.9	600	75	H_2O:ACN (50:50 v/v)	Mixed	5375
AN5	A	2.9	600	75	H_2O:ACN (50:50 v/v)	Single	5375
Levo5	B	2.8	120 - 250	75	H_2O:ACN (50:50 v/v)	Single	1075-2240
Levo6	B	3	120 - 250	75	H_2O:ACN (50:50 v/v)	Single	1075-2240
Levo7	B	3	120 - 250	75	H_2O:ACN (50:50 v/v)	Single	1075-2240
Levo8	B	2.9	120 - 250	75	H_2O:ACN (50:50 v/v)	Single	1075-2240
Levo9	B	2.9	120 - 250	75	H_2O:ACN (50:50 v/v)	Single	1075-2240

Table S3. Estimation of electrospray (ES) parent droplet size and number concentrations using the median of the ES flow rate. The estimated ES parent droplet number flux was used for the estimation of coagulation rates between ES droplets and particles.

Index no.	**ES Flow Rate, Q (nL min^{-1})**	**Estimated ES Parent Droplet Size, D_{ES} (μm)**	**Estimated ES Parent Droplet Number Flux N_{ES}, Q/D_{ES} (s^{-1})**
Levo1 + AN1	354	0.70	$32.9 \cdot 10^6$
Levo2 + AN2	22655	5.66	$4 \cdot 10^6$
Levo3	1792-3584	1.59	$14.2 - 28.3 \cdot 10^6$
Levo4	1309-2617	1.45	$13.7 - 27.3 \cdot 10^6$
AN3	1792-3584	1.59	$14.2 - 28.3 \cdot 10^6$
AN4 + Suc1	5375	2.76	$8.1 \cdot 10^6$
AN5	5375	2.76	$8.1 \cdot 10^6$
Levo5	1075-2240	1.53	$9.6 - 20 \cdot 10^6$
Levo6	1075-2240	1.53	$9.6 - 20 \cdot 10^6$
Levo7	1075-2240	1.53	$9.6 - 20 \cdot 10^6$
Levo8	1075-2240	1.53	$9.6 - 20 \cdot 10^6$
Levo9	1075-2240	1.53	$9.6 - 20 \cdot 10^6$

The coagulation coefficients K_{12} were calculated using the Fuchs form of the Brownian coagulation coefficient (Seinfeld and Pandis, 2016).

$$K_{12} = 2\pi(D_1 + D_2)(D_{p1} + D_{p2})\left(\frac{D_{p1}+D_{p2}}{D_{p1}+D_{p2}+2(g_1^2+g_2^2)^{1/2}} + \frac{8(D_1+D_2)}{(\bar{C}_1^2+\bar{C}_2^2)^{\frac{1}{2}}(D_{p1}+D_{p2})}\right)^{-1} \quad \text{(Eq. S6)}$$

where

$$\bar{C}_i = \left(\frac{8k_BT}{\pi m_i}\right)^{1/2}$$

$$l_i = \frac{8D_i}{\pi\bar{C}_i}$$

$$g_i = \frac{\sqrt{2}}{3D_{pi}l_i}\left[\left(D_{pi} + l_i\right)^3 - \left(D_{pi}^2 + l_i^2\right)^{3/2}\right] - D_{pi}$$

$$D_i = \frac{k_BTC_c}{3\pi\mu D_{pi}},$$

and C_c is the Cunningham slip correction factor. D_{p1} is denoted as D_{ES} (Eq. S5, Table S3) with the density of the electrospray solution (Table S1) and D_{p2} is denoted as the mid-size of the measured *j*-th bin of the size-selected particle size distribution with the density of the particle. For clarity, K_{12} is hereafter referred to as $K_{ES,J}$.

The coagulation rate J_{12} between the ES parent droplets and analyte particles can be calculated as

$$J_{12} = N_{ES}\sum_{j=1}^{\infty} K_{ES,J}N_J \quad \text{(Eq. S7)}$$

where N_{ES} is the estimated ES parent droplet number flux (Table S3), $K_{ES,J}$ is the calculated Brownian coagulation coefficient (Eq. S6) and N_j is the number concentration of the measured *j*-th bin of the size-selected analyte particle size distribution. Please note that Eq. S7 does not take into account of potential inhomogeneity of ES droplet and particle distributions during coagulation.

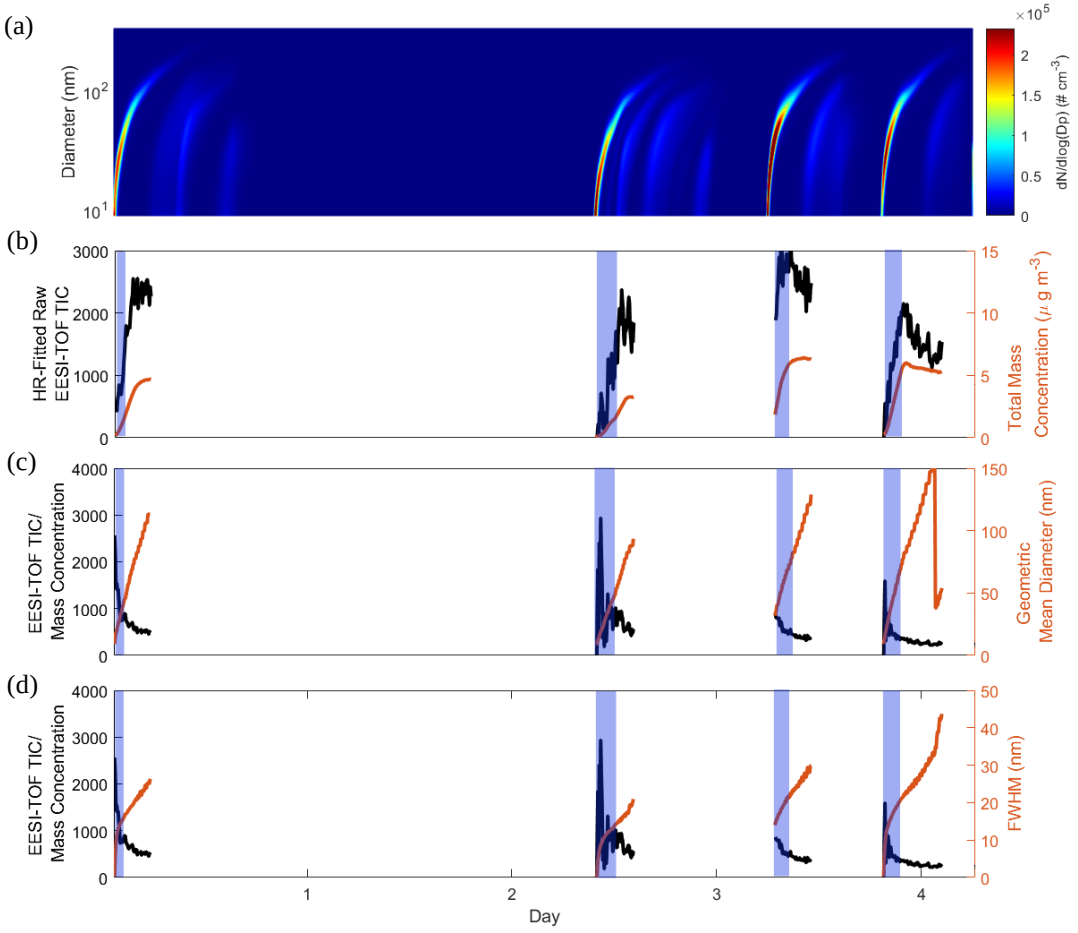

Figure S8. SOA formation experiments in the CLOUD chamber. (a) SMPS measurements of the number-weighted size distribution. (b) Raw EESI-TOF total ion counts (TIC) after high-resolution peak fitting and total mass concentrations measured by the SMPS with an effective mass density of 1.3 g cm^{-3}. (c) EESI-TOF TIC normalized by the mass concentration measured by the SMPS, and the geometric mean diameter. (d) EESI-TOF TIC normalized by the mass concentration measured by the SMPS, and the full width at half maximum (FWHM) of the volume-weighted size distribution. Shaded areas depict the period during new particle formation events where EESI size-dependent sensitivities are observed as shown in Figure 3.

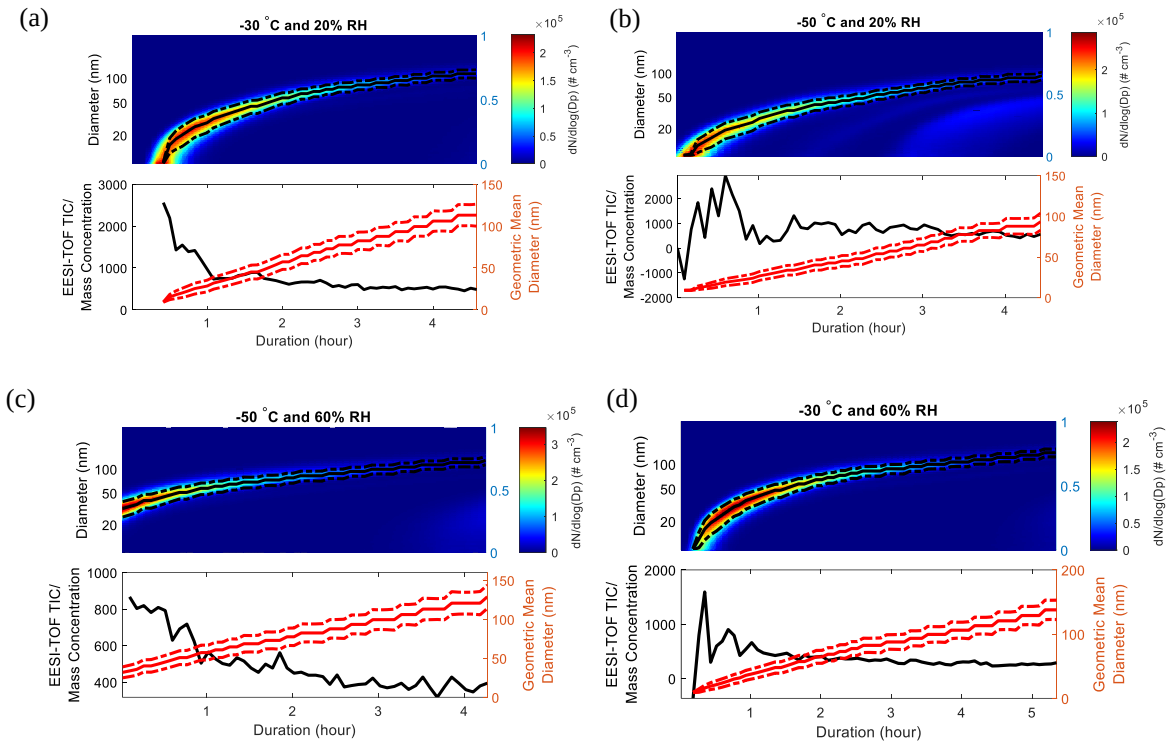

Figure S9. (Top sub-panel) SMPS size distributions and (bottom sub-panel) sum of the high-resolution fitted ions of EESI normalized by the mass concentration measured by the SMPS for α-pinene (AP) SOA formation experiments in the CLOUD chamber at four different conditions. (a) AP SOA formation at -30 °C and 20% relative humidity (RH). (b) AP SOA formation at -50 °C and 20% RH. (c) AP SOA formation at -50 °C and 60% RH. (d) AP SOA formation at -30 °C and 60% RH.

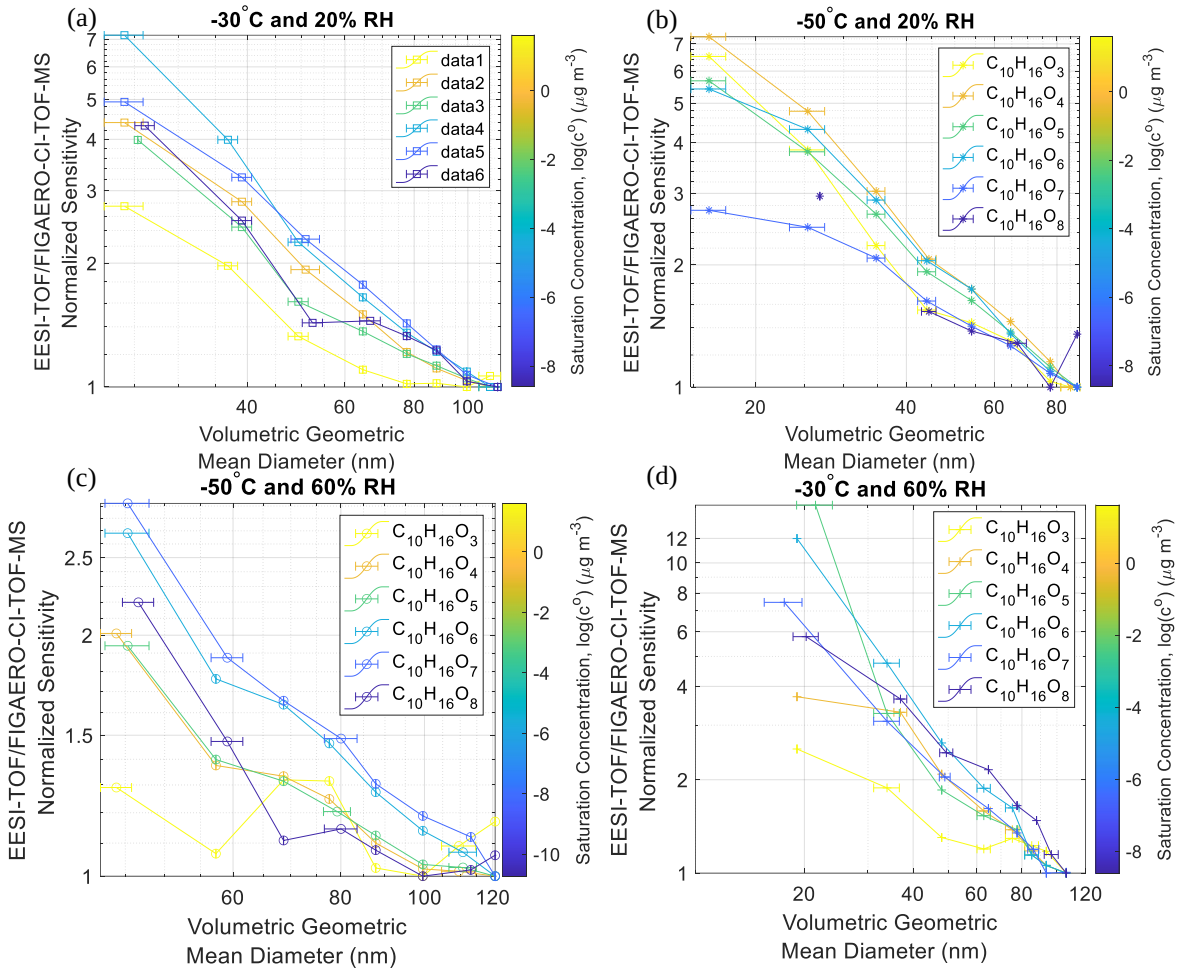

Figure S10. Measurements of $C_{10}H_{16}O_{3\text{-}8}$ in the particle phase. EESI-TOF to FIGAERO-CI-TOF-MS normalized sensitivity for AP SOA formation experiments in the CLOUD chamber at four different conditions.

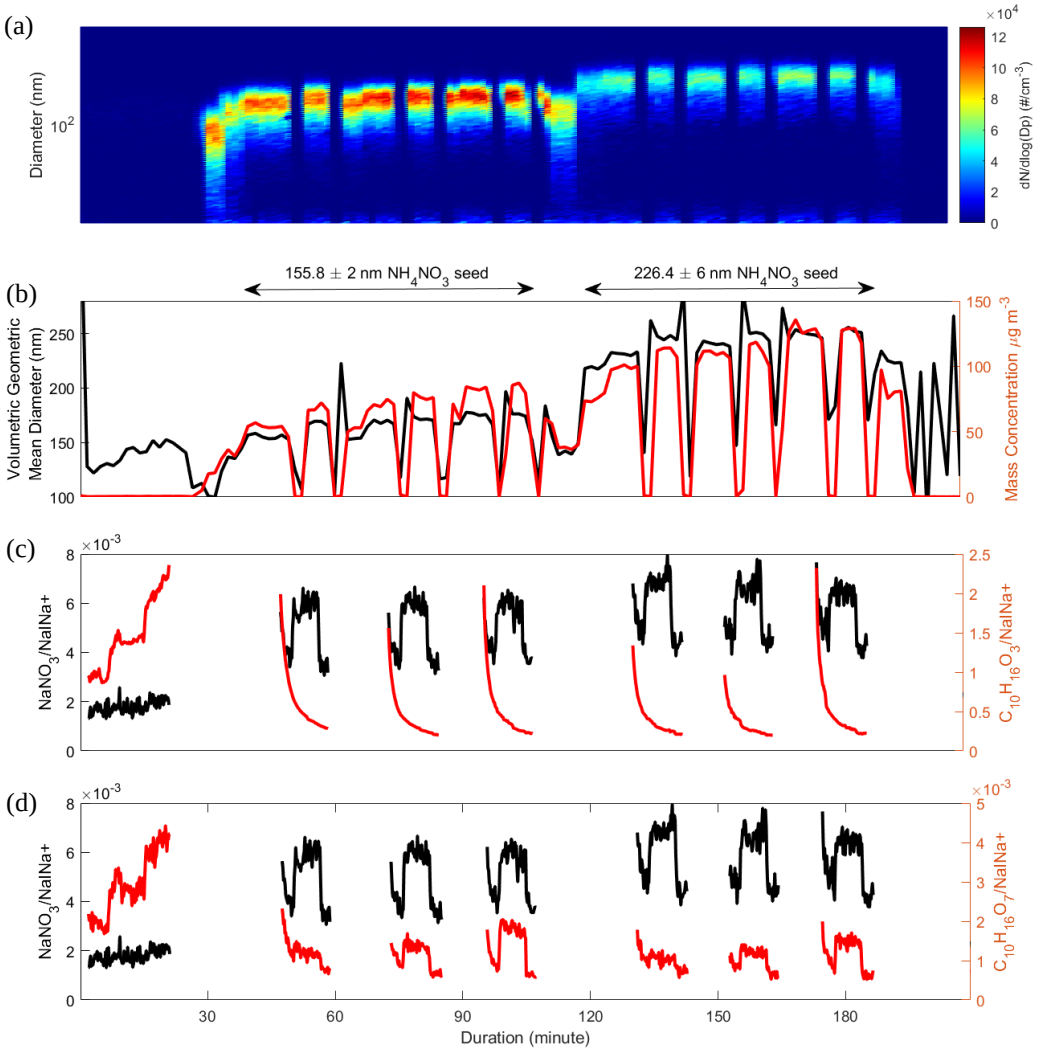

Figure S11. Coating of NH_4NO_3 particles using oxidation products of α-pinene ozonolysis. (a) Size distribution of the coated NH_4NO_3 particles. (b) Volume weighted geometric mean diameter and mass concentration measured by the SMPS. (c) Signals of NH_4NO_3 particles and particle-phase $C_{10}H_{16}O_3$ molecules. (d) Signals of NH_4NO_3 particles and particle-phase $C_{10}H_{16}O_8$ molecules.

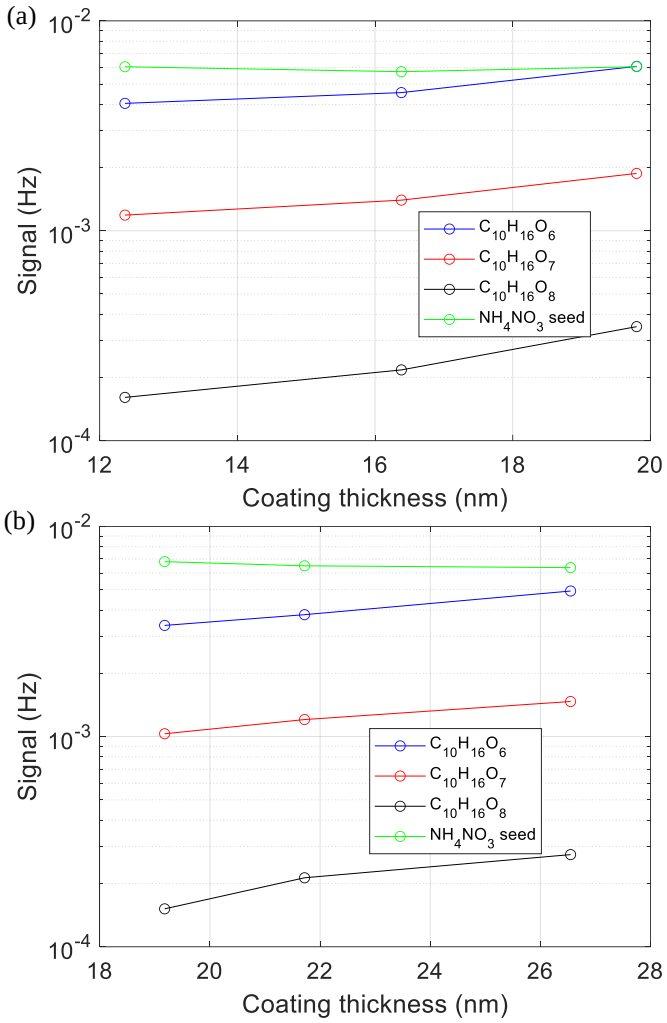

165

Figure S12. Absolute changes of NH_4NO_3 and $C_{10}H_{16}O_{6\text{-}8}$ as a function of the coating thickness for two different NH_4NO_3 particle core sizes of (a) 156 nm and (b) 226 nm after normalization to the most abundant electrospray ion adduct $[NaI+Na]^+$.

References

Gañán-Calvo, A. M., López-Herrera, J. M., Rebollo-Muñoz, N. and Montanero, J. M.: The onset of electrospray: The universal scaling laws of the first ejection, Sci. Rep., 6(1), 1–9, doi:10.1038/srep32357, 2016.

Gañán-Calvo, A. M., López-Herrera, J. M., Herrada, M. A., Ramos, A. and Montanero, J. M.: Review on the physics of electrospray: From electrokinetics to the operating conditions of single and coaxial Taylor cone-jets, and AC electrospray, J. Aerosol Sci., 125, 32–56, doi:10.1016/j.jaerosci.2018.05.002, 2018.

Kirkby, J., Curtius, J., Almeida, J., Dunne, E., Duplissy, J., Ehrhart, S., Franchin, A., Gagné, S., Ickes, L., Kürten, A., Kupc, A., Metzger, A., Riccobono, F., Rondo, L., Schobesberger, S., Tsagkogeorgas, G., Wimmer, D., Amorim, A., Bianchi, F., Breitenlechner, M., David, A., Dommen, J., Downard, A., Ehn, M., Flagan, R. C., Haider, S., Hansel, A., Hauser, D., Jud, W., Junninen, H., Kreissl, F., Kvashin, A., Laaksonen, A., Lehtipalo, K., Lima, J., Lovejoy, E. R., Makhmutov, V., Mathot, S., Mikkilä, J., Minginette, P., Mogo, S., Nieminen, T., Onnela, A., Pereira, P., Petäjä, T., Schnitzhofer, R., Seinfeld, J. H., Sipilä, M., Stozhkov, Y., Stratmann, F., Tomé, A., Vanhanen, J., Viisanen, Y., Vrtala, A., Wagner, P. E., Walther, H., Weingartner, E., Wex, H., Winkler, P. M., Carslaw, K. S., Worsnop, D. R., Baltensperger, U. and Kulmala, M.: Role of sulphuric acid, ammonia and galactic cosmic rays in atmospheric aerosol nucleation, Nature, 476(7361), 429–435, doi:10.1038/nature10343, 2011.

Lee, C. P., Riva, M., Wang, D., Tomaz, S., Li, D., Perrier, S., Slowik, J. G., Bourgain, F., Schmale, J., Prevot, A. S. H., Baltensperger, U., George, C. and El Haddad, I.: Online Aerosol Chemical Characterization by Extractive Electrospray Ionization-Ultrahigh-Resolution Mass Spectrometry (EESI-Orbitrap), Environ. Sci. Technol., 54(7), 3871–3880, doi:10.1021/acs.est.9b07090, 2020.

Lopez-Hilfiker, Pospisilova, V., Huang, W., Kalberer, M., Mohr, C., Stefenelli, G., Thornton, J. A., Baltensperger, U., Prevot, A. S. H. and Slowik, J. G.: An extractive electrospray ionization time-of-flight mass spectrometer (EESI-TOF) for online measurement of atmospheric aerosol particles, Atmos. Meas. Tech., 12(9), 4867–4886, doi:10.5194/amt-12-4867-2019, 2019.

Seinfeld, J. H. and Pandis, S. N.: Atmospheric Chemistry and Physics: From Air Pollution to Climate Change, 3rd ed., Wiley., 2016.